Structural flexibility of the tetanus neurotoxin revealed by crystallographic and solution scattering analyses

Chun-ming Zhang [a,1,*], Yoshihiro Imoto [a,1], Takaaki Hikima [b], Tsuyoshi Inoue [a,*]

[a] *Graduate School of Pharmaceutical Science, Osaka University, Suita, 565-0871 Osaka, Japan*
[b] *Advanced Photon Technology Division, RIKEN SPring-8 Center, Sayo-gun, 679-6148, Japan*

ARTICLE INFO

ABSTRACT

Although the tetanus neurotoxin (TeNT) delivers its protease domain (LC) across the synaptic vesicle lumen into the cytosol via its receptor binding domain (H_C) and translocation domain (H_N), the molecular mechanism coordinating this membrane translocation remains unresolved. Here, we report the high-resolution crystal structures of full-length reduced TeNT (rTeNT, 2.3 Å), TeNT isolated H_N (TeNT/iH_N, 2.3 Å), TeNT isolated H_C (TeNT/iH_C, 1.5 Å), together with the solution structures of TeNT/iH_N and beltless TeNT/iH_N (TeNT/blH_N). TeNT undergoes significant domains rotation of the H_N and LC were demonstrated by structural comparison of rTeNT and non-reduced-TeNT (nrTeNT). A linker loop connects the H_N and H_C is essential for the self-domain rotation of TeNT. The TeNT-specific C869-C1093 disulfide bond is sensitive to the redox environment and its disruption provides linker loop flexibility, which enables domain arrangement of rTeNT distinct from that of nrTeNT. Furthermore, the mobility of C869 in the linker loop and the sensitivity to redox condition of C1093 were confirmed by crystal structure analysis of TeNT/iH_C. On the other hand, the structural flexibility of H_N was investigated by crystallographic and solution scattering analyses. It was found that the region (residues 698–769), which follows the translocation region had remarkable change in TeNT/iH_N. Besides, the so-called belt region has a high propensity to swing around the upper half of TeNT/iH_N at acidic pH. It provides the first overview of the dynamics of the Belt in solution. These newly obtained structural information that shed light on the transmembrane mechanism of TeNT.

1. Introduction

The tetanus neurotoxin (TeNT), also known as tetanospasmin, is a debilitating and fatal poison produced by the obligate anaerobic bacterium *Clostridium tetani* (*C. tetani*). TeNT is the causative agent of tetanus, a disease caused by contamination of deep flesh wounds with the spores of *C. tetani* whose natural habitat is soil and enteric canals of various animals (Bruggemann et al., 2003). The spores sprout and grow into bacteria that produce TeNT in the necrotic and anaerobic wound. TeNT is initially taken up at the neuromuscular junction (NMJ) by endocytosis and invades motor neurons (Bercsenyi et al., 2014). The toxin is then transported retrogradely into the spinal cord of the central neuron (Schwab, 1979). Thereafter, TeNT cleaves vesicle-associated membrane protein 2 (VAMP2), which is a member of the soluble *N*-ethylmaleimide-sensitive factor attachment protein receptor (SNARE) (Schiavo et al., 1992). VAMP2 forms a ternary complex with the plasma membrane to promote fusion of synaptic vesicles (Südhof and Jahn, 1991). Therefore, disrupting formation of the SNARE complex by TeNT blocks neurotransmitter release. As a result, the function of inhibitory interneurons is lost, leading to spasms and stiffness in muscles. A horrible outcome of tetanus poisoning is that the patient is fully conscious during such complications and experiences extreme pain (Rossetto et al., 2019). There are no specific drugs to cure tetanus. Although cases of tetanus are rare in developed countries because of the available tetanus vaccine, it remains a major threat to people living in low-income countries where easy access to the tetanus vaccine is not possible, routine immunization programs do not exist, and clean and safe birth practices are not established (WHO, Protecting all against tetanus, 2019).

The ability of TeNT to specifically and effectively target the central nervous system (CNS) by retrograde axonal transport, and deliver its protease domain (LC) into the cytosol across the synaptic vesicle lumen,

has raised interest in using TeNT as a delivery vehicle to transport drugs into neurons. Numerous applications have been performed using the receptor binding domain (H_C) of TeNT (TeNT/H_C), including the TeNT/H_C-mediated anti-inflammatory effect in amyotrophic lateral sclerosis (ALS) (Moreno-Martinez, 2020), a TeNT/H_C-mediated tracer for the study of the structure and organization of the nervous system (Kissa, 2002; Maskos et al., 2002), TeNT/H_C-mediated neuronal targeting of metabolic enzymes (Dobrenis et al., 1992) and TeNT/H_C-mediated delivery of neurotrophins (Bordet et al., 2001; Rind, 2005; Payne et al., 2006; Roux et al., 2006). The use of TeNT as a therapeutic tool requires the removal of its toxicity. The non-toxic TeNT/H_C is provided either as a protein fragment or fusion protein, which binds the pre-synaptic motor neuron terminal and facilitates retrograde axonal transport of the desired therapeutic molecule to the CNS (Toivonen et al., 2010). These applications involve either mutation of key residues or construction of hybrid proteins with TeNT/H_C (Coen et al., 1997) to control the receptor binding step and regulate the efficacy of the toxin in the CNS. A further goal of TeNT engineering involves expanding its use to expletive cell types, such as non-neuronal cells, which can be carried out by replacing the H_C with a targeted transmission that binds to a specific cell type. Noteworthily, in the later study, it was shown that low doses wild type TeNT are safe and present therapeutic effects of spinal cord injury (SCI) (Hesse et al., 2020). Further improvements to the pharmacological properties of TeNT, such as lower immunogenicity and higher efficacy, are highly desired and should increase the medical use of TeNT. Because most current TeNT applications are based on the molecular structure of TeNT, multifaceted structural analysis and elucidation of the molecular mechanism of TeNT entry into cells in detail should lead to new concepts and promote TeNT-based therapeutics.

TeNT is produced as a 150 kDa single chain polypeptide and cleaved by an endogenous protease to form a di-chain composed of the 50 kDa light chain (LC) and the 100 kDa heavy chain (HC) (Eisel et al., 1986). A disulfide bond links the LC and HC to each other. The LC is a zinc ion endopeptidase domain that is delivered across the synaptic vesicle lumen into the neuronal cytosol where VAMP2 is cleaved (Pirazzini et al., 2011; Schiavo et al., 2000). The HC is further divided into the C-terminal (H_C) and N-terminal (H_N) domains. The H_C is a ligand binding domain that recognizes polysialoganglioside (PSG) (Rummel et al., 2003; Chen et al., 2009) and synaptic vesicle proteins 2 (SV2) (Yeh et al., 2010) on the presynaptic membrane. It has also been reported that the H_C interacts with nidogens at the NMJ (Bercsenyi et al., 2014). The H_N assists with synaptic vesicle lumen translocation of the LC (Fischer and Montal, 2013), and is thus also called the translocation domain. The H_N has a characteristic belt region that wraps around the LC, and the movement of the Belt in solution has yet to be demonstrated, and the *in vivo* relevance of it for the membrane translocation of the LC remains to be established. The beltless isolated H_N from the botulinum neurotoxin A (BoNT/A) forms a pH-independent ion channel (Fischer et al., 2012). The H_N contains a loop region parallel with the long α-helices that is rich in hydrophobic residues and is termed the channel-forming motif or translocation region because a synthetic peptide corresponding to this region forms a cation-selective channel embedded in the membrane (Oblatt-Montal et al., 1995). A recent study of the beltless isolated H_N from BoNT/A showed that buried α-helices (BoNT-switch), which structurally follow the translocation region in the H_N, transform into a β-hairpin structure under acidic pH conditions and this transformation facilitates membrane insertion of the H_N (Lam et al., 2018). Therefore, it is hypothesized that these regions enable the H_N to approach the membrane. Masuyer Geoffrey and co-works have described the pH-mediated domain rearrangements of non-reduced TeNT (nrTeNT), in which TeNT forms different structures at pH > 6.3, pH 6.3–5.5 and pH < 5.5 (Masuyer et al., 2017). The structure also reveals that an H_N–H_{CN} linker contains the C869–C1093 disulfide bridge, which is a unique feature of TeNT. However, the function of this tetanus-specific disulfide bond during TeNT poisoning is poorly understood.

Two models for membrane translocation of the LC mediated by the H_N on the synaptic vesicle lumen have been proposed: the channel model and cleft model. For the channel model, the H_N undergoes a conformational change upon synaptic vesicle acidification, enabling it to soak into the vesicle lumen, leading to the formation of a channel that escorts the partially unfolded LC across the synaptic vesicle lumen (Montal, 2009). For the cleft model, structural rearrangement of the H_N and LC and lipids upon acidification of the synaptic vesicle and lipid interactions, which further facilitates the interaction between the translocation region and lipid bilayer, leads to the formation of a cleft. The LC is postulated to cross the vesicle lumen through this cleft (Rossetto et al., 2014).

Despite enthusiastic structural studies on TeNT and BoNTs, the molecular mechanism underlying the cooperation of each domain during membrane translocation of LC remains unresolved (Dong et al., 2019). To better understand the action of TeNT during membrane translocation, especially the activation of the H_N, we have determined the crystal structures of full-length reduced TeNT (rTeNT) and TeNT isolated H_N (TeNT/iH_N) as well as the highest-resolution crystal structure of TeNT isolated H_C (TeNT/iH_C). Small angle X-ray scattering combined with size exclusion chromatography (SEC-SAXS) of TeNT/iH_N and beltless TeNT/iH_N (termed TeNT/blH_N) has also been performed. We propose an up-to-date membrane translocation mechanism of TeNT based on the newly obtained structural data, providing new concept that should enable novel drug design to meet specific medical need.

2. Results

2.1. Rotation of the reduced TeNT Domains.

To elucidate conformational changes to rTeNT, the crystal structure of TeNT was determined after treatment with tris (2-carboxyethyl) phosphine (TCEP), a reductant present in the purification buffer. For safety reasons, a catalytically inactive and non-toxic full-length TeNT was used, which has several mutations to the catalytic site of the LC (H233A/E234Q/H237A/Y375F). The pure and intact full-length rTeNT was demonstrated by SDS-PAGE (Fig. S1A). The crystal structure of rTeNT was determined at 2.3 Å resolution with well-defined electron density for the macromolecule (Table 1, Fig. S1B). The asymmetric unit contains one molecule of rTeNT and consists of the C-terminal subdomain of H_C (H_{CC}), N-terminal subdomain of H_C (H_{CN}), H_N, Belt and LC (Fig. 1A).

Structural comparison between the crystal structure of nrTeNT in complex with a ganglioside GD1a (PDB ID: 5N0B) (Fig S2A) and rTeNT yielded root-mean-square-deviation (rmsd) values for the H_C, H_N and LC of 0.55 Å (for 395 Cα pairs), 0.75 Å (for 333 Cα pairs), and 0.45 Å (for 394 Cα pairs), respectively. Except for a few changes in interactions between the H_C and H_N (*vide infra*), the overall folds of each domain are very similar between rTeNT and nrTeNT. However, the H_N and LC in rTeNT show a domain rotation when compared with those in nrTeNT. Fig. 1B and 1C show superimposition of the H_{CC} subdomain (rTeNT$^{1111–1315}$) from rTeNT and nrTeNT. The H_N of rTeNT (rTeNT/H_N) is rotated approximately 125 degrees when K697 and W726 are used as a rotation marker and rotation center, respectively (Fig. 1B). The receptor binding site and the translocation region are at two opposite ends of the molecule in rTeNT, whereas they point in the same direction (membrane) in the nrTeNT structure.

Two disulfide bonds are reported in the previous 2.6 Å resolution structure of nrTeNT. One is C439–C467, which connects the H_N and LC, and is conserved among clostridial neurotoxins (CNTs). The other is C869–C1093, which connects the H_N and H_{CN} via two flexible linker loops. Sequence alignment of the H_N and H_{CN} linker for CNTs revealed that the linker has a unique cysteine residue (C869) in TeNT (Fig. S2B). C439–C467 is present in rTeNT and stabilized by β strands formed between the LC and Belt in the H_N, as observed in nrTeNT (Fig. S2C). In contrast, we did not observe the C869–C1093 disulfide bond in the present rTeNT structure despite the higher resolution of 2.3 Å (Fig. S2D).

Table 1
Data collection and refinement statistics of the crystal structures.

Data collection			
	rTeNT	H_N	H_C
Resolution range (Å)*	48.28–2.27 (2.32–2.27)	47.78–2.34 (2.43–2.34)	50.0–1.50 (1.53–1.50)
Space group	P3₁21	P2₁2₁2₁	P2₁2₁2₁
Unit cell a, b, c (Å)	145.54, 145.54, 129.04	39.60, 107.12, 211.41	66.71, 79.39, 89.75
No. total/unique reflections*	475,310/72,360	251,166/38,647	505,104/75,134
R_{merge} (%)*	12.6 (103)	7.2 (95.0)	7.3 (49.7)
$R_{p.i.m.}$ (%)*	5.3 (44.6)	3.1 (39.5)	3.0 (25.5)
I/σ (I)*	10.7 (1.7)	11.5 (1.7)	26.9 (2.68)
$CC_{1/2}$*	0.997 (0.634)	0.998 (0.888)	0.941 (0.795)
Completeness (%)*	99.2 (94.7)	99.3 (95.2)	97.6 (89.4)
Redundancy*	6.6 (5.9)	6.5 (6.6)	6.7 (4.6)
Refinement			
Resolution range (Å)	48.28–2.27	38.92–2.34	44.41–1.50
R_{work} (%)/R_{free} (%)	18.6/23.3	20.9/25.3	12.2/16.3
Rmsd bonds/angles (Å, ˚)	0.003/0.905	0.009/1.10	0.009/1.436
No. AA	1299	812	451
No. atoms			
Protein	10,470	4808	3861
Ligand	37	0	20
Ion	4	0	1
Water	785	81	531
B value (Å)			
R_{mean}	59.66	77.0	24.12
R_{Wilson}	38.3	58.1	12.8
Protein atoms	59.3	78.1	22.3
Water	64.4	63.7	37.0
Other atoms	79.3	–	35.9
Ramachandran plot (%)			
Favored	97.34	96.43	95.18
Allowed	2.66	3.57	4.82
Disallowed	0	0	0
PDB ID	7BY5	7BXX	7BY4

*Values in parentheses are for highest-resolution shell.

Although both disulfide bridges are present on the molecular surface, C869–C1093 appears to be more sensitive to the redox environment than C439–C467 and is possibly absent in the presence of TCEP. Superimposition of the H_C and H_N in rTeNT onto those in nrTeNT revealed that only 11 residues (SKNLDCWVDNE) in the H_N and H_{CN} linker are essential for the H_N rotation. Remarkably, C869 is positioned in the middle of the segment. Regardless of the C869 is invisible in the electron density map, the SDS-PAGE result of rTeNT from crystals demonstrated that rTeNT remains intact (full-length) in crystals and the C869 is located on the flexible linker loop (Fig. S2E). Therefore, the disruption of the C869–C1093 disulfide bond provides linker loop flexibility, which enables domain arrangement of rTeNT distinct from that of nrTeNT.

The LC of rTeNT (rTeNT/LC) is rotated around 120 degrees when the fragment (136–153) and W726 are used as a rotation marker and rotation center, respectively (Fig. 1C). The LC is wrapped by the Belt of H_N to form a single rigid LC–H_N structure. The domain rotation did not affect the overall LC structure (Fig. S3A, B). A loop (residues 333–339, termed the 333loop) in nrTeNT (after rotation) fits well with the corresponding region in rTeNT (before rotation). The 333loop is well conserved in CNTs (Fig. S3C) and contains several negatively charged residues (Fig. S3D). Removed

Overall, the results described about rotation of domains in TeNT occur after anchoring to the membrane by the H_{CC}. This rotation likely to be regulated by the C869–C1093 disulfide bond via the H_N–H_{CN} linker. As a result, the H_N and LC locate closer to the presynaptic membrane along with the translocation region.

2.2. Crystal structure of the isolated H_N from TeNT.

The crystal structure of the TeNT/iH_N was determined to unravel how the H_N undergoes conformational changes in the absence of the H_C and LC. In the present work, C467 in TeNT/iH_N was mutated to serine (C467S) to prevent unwanted dimer formation induced by a disulfide bond (Fig. S4A). The crystal structure of TeNT/iH_N at pH 6.6 was refined to 2.3 Å resolution (Table 1) and represents the first TeNT/iH_N structure determined. The asymmetric unit contains two molecules of TeNT/iH_N related by a non-crystallographic two-fold axis (Fig. S4B). The H_N consists of two long coiled-coil helices with additional short helices (Fig. 2A). The buried α-helices region in H_N (residues 629–668), which corresponds to the BoNT-switch, was identified. The translocation region (residues 669–697) follows after this region (hereinafter termed H_N-switch). The electron density of the Belt (residues 459–563) was not observed in both chains. Superimposition of rTeNT/$H_N^{564-864}$ onto TeNT/iH_N (rmsd of 1.2 Å for 285 Cα pairs) shows that the Belt in TeNT/iH_N could not adopt the conformation observed in rTeNT because of steric hindrance with neighboring molecules in the crystal packing (Fig. 2B). Structural differences between chain A/B of TeNT/iH_N and the H_N of rTeNT were found at K736 and Y739, which respectively interact with the Belt and LC in rTeNT (Fig. 2C). In rTeNT, K736 formed hydrogen bonds with the carbonyl O atoms of E473 and L475. The hydroxyl group of Y739 formed a hydrogen bond with the amide N atom of M378. In chain A of TeNT/iH_N, the N_ζ atom of K736 and the hydroxyl group of Y739 moved by 5.2 and 8.0 Å, respectively, from each position in rTeNT. The change in the chi 1 and chi 2 angle of Lys736 were from −142.9 to −172.6 degrees, 77.5 to −178.2 degrees, respectively. And the change in the chi 1 angle of Tyr739 was from −76.4 to 171.0 degrees. This result demonstrates that in the absence of the H_C and LC induces structural changes of the H_N. Superimposition of the N-terminal region of α₇ (residues 701–731) and the C-terminal region of α₈ (801–836) in rTeNT, nrTeNT and TeNT/iH_N reveals significant movement around residues 762–769, which is called the *cis*-loop region and involved in LC membrane translocation (Zuverink et al., 2020) (Fig. S5A). Distances from the Cα atom of K768 in rTeNT/H_N to those of nrTeNT/H_N, TeNT/iH_N chain A and TeNT/iH_N chain B are 3.2, 5.9 and 8.9 Å, respectively (Fig. S5B). Moreover, while E698, K699 and I700 form a helix in rTeNT and TeNT/iH_N, these residues form a loop in nrTeNT (Fig. S5C).

2.3. Size exclusion chromatography combined with small angle X-ray scattering (SEC-SAXS) measurements

To address the movement of the Belt in solution, which was not observed in the crystal structure, the solution structure of TeNT/iH_N (459–864) was investigated by SEC-SAXS. For comparison, we conducted additional experiments using TeNT/blH_N (residues 560–864, "bl" indicates beltless). The TeNT/blH_N was purified successfully as shown in Fig. S4A. Frames across the peak of the SEC peak were selected for averaging that yield the scattering profile (Fig. S6A, B). The scattering profiles of TeNT/iH_N and TeNT/blHN with their Guiner plot revealed no signs of aggregation (Fig. S6C). The radius of gyration (R_g) was 30.35 and 29.31 Å, and the maximum intramolecular distance (D_{max}) was 121.32 and 112.16 Å for TeNT/iH_N and TeNT/blH_N, respectively (Table 2) (Fig. S6D). The D_{max} value of TeNT/blH_N is consistent with 110 Å, the length of the large helix of H_N. The experimental molecular weights of TeNT/iH_N and TeNT/blH_N were 44.0 and 32.6 kDa, respectively (Table 2). These values are consistent with the molecular weights of 46.6 and 35.2 kDa for TeNT/iH_N and TeNT/blH_N, respectively (Fig. S4A). The Kratky plot revealed a parabolic shape indicative that both main components of the protein samples adopted folded states (Fig. S6E). The crystal structure model of rTeNT/H_N (residues 564–864) fitted well into the bent rod part of the DAMMIN model of TeNT/iH_N. However, the original conformation of the Belt (light blue) in rTeNT did not fit with the beads model (Fig. 3A, B). Conversely, non-negligible unfitted additional parts were observed around rTeNT/H_N.
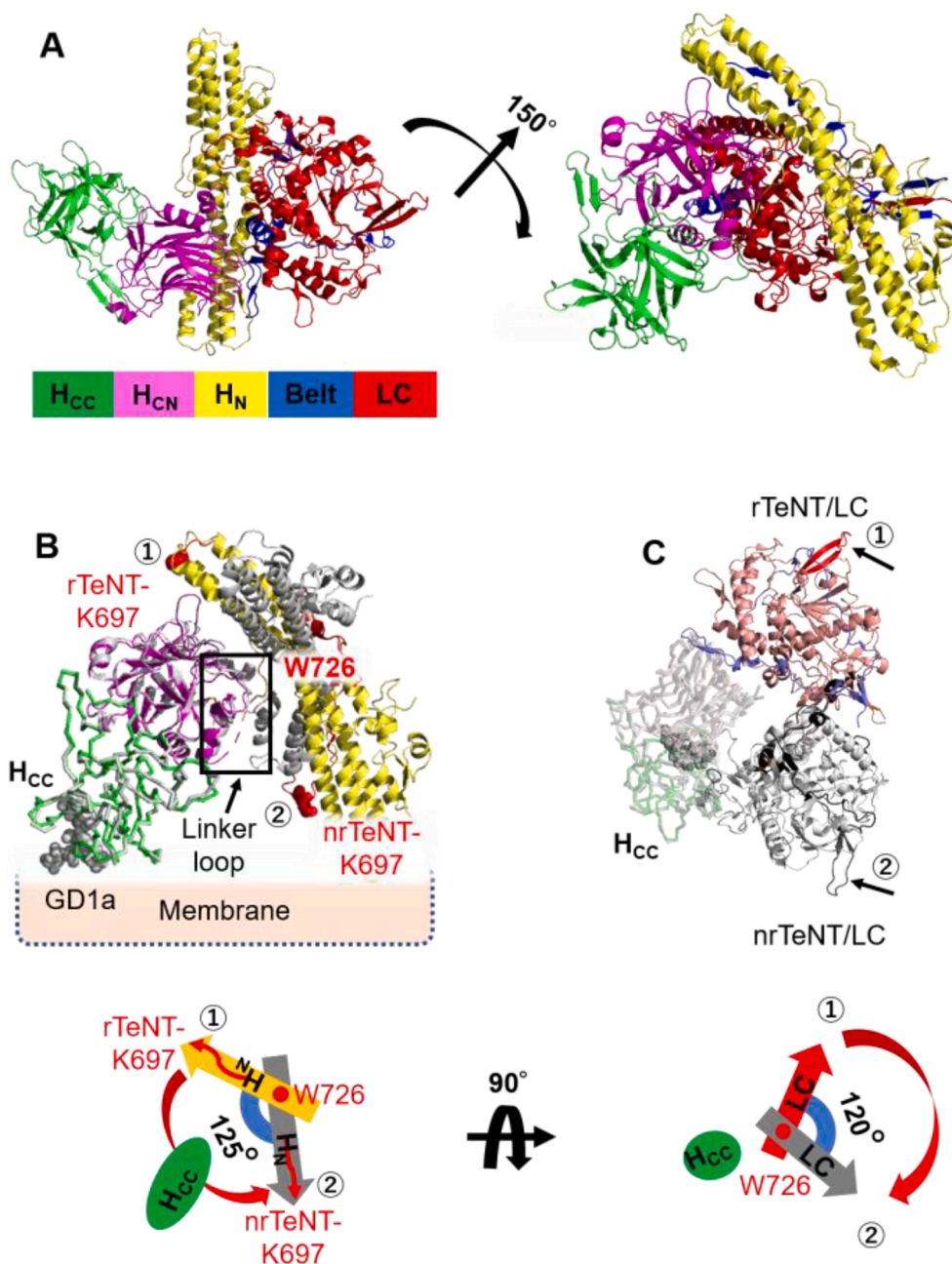
Fig. 1. Rotation of domains in reduced TeNT (rTeNT). (A) Crystal structure of the reduced TeNT (rTeNT). Left, the rTeNT molecule consists of the C-terminal subdomain (H_{CC}, green), N-terminal subdomain (H_{CN}, magenta), H_N (yellow), Belt (blue) and LC (red). Right, cartoon presentation of the domain organization of rTeNT on the membrane. (B) Rotation of the H_N. Superimposition of rTeNT[1111–1315] (green, ribbon) and the corresponding domain of nrTeNT (gray, ribbon). The rotation angle between rTeNT-K697 and nrTeNT-K697 is ∼ 125 degrees. As K697 (red spheres) is a rotation marker, W726 is a vertex of the angle. The linker loop is highlighted by the black box. The side of GD1a shows the position of the membrane. Cartoon model of the H_N rotation is shown (bottom left). The translocation region and W726 are shown as the red curved arrow and red dot, respectively. (C) Rotation of the LC. The rotation angle between rTeNT/LC (salmon) and nrTeNT/LC (gray) is ∼ 120 degrees. The Belt in rTeNT and nrTeNT is shown in light blue and black, respectively. Peptide fragment (136–153) (red and gray in rTeNT/LC and nrTeNT/LC, respectively) is a rotation marker, and W726 is a vertex of the angle. Cartoon model of the LC rotation is shown (bottom right). (For interpretation of the references to colour in this figure legend, the reader is referred to the web version of this article.)

Thus, we tried to fit an averaged theoretical scattering intensity derived from an ensemble of conformations to the experimental SAXS data by the ensemble optimization method (EOM) (Fig. S6F). Fitting EOM models into the DAMMIN model of TeNT/iH_N revealed that those positions represent the location of the Belt in the solution structure of TeNT/iH_N, indicating that the Belt shows highly flexible structural characteristics (Fig. 3A, Fig. S6G). Additionally, the crystal structure model, which was generated from the crystal structure of rTeNT (residues 564–864), corresponding to the TeNT/blH_N fitted well to the rod-like shape beads model of TeNT/blH_N, which strongly supports the concept that the Belt in TeNT/iH_N is likely to swing around the upper half of TeNT/iH_N in solution (Fig. 3C, D, Fig. S6H).

2.4. Crystal structure of the isolated H_C from TeNT

To further understand the structural characteristics of TeNT/iH_C (Fig. S7A), especially the action of the C869–C1093 disulfide bond, the crystal structure of TeNT/iH_C without TCEP treatment was determined at 1.5 Å resolution (Table 1), which is the highest resolution structure solved of this domain (Fig. S7 B). The asymmetric unit contains one molecule of TeNT/iH_C. The C869–C1093 disulfide bond was absent, and C869 was not observed in TeNT/iH_C. In contrast, C1093 had oxidized to form S-hydroxycysteine (Fig. S7C), despite the short life of the sulfenic acid intermediate. These results suggest that C869 in the H_N–H_{CN} linker has high mobility, and C1093 in TeNT/iH_C is sensitive to redox conditions, which may lead to the disruption of the C869–C1093 disulfide bond.

Earlier studies showed that the H_C of TeNT binds gangliosides via two ganglioside binding sites (GBS), the "W" pocket and the "R" pocket (Rummel et al., 2003; Chen et al., 2009). Our TeNT/iH_C structure shows that a buffer component, bis-(2-hydroxyethyl) aminotris (hydroxymethyl)methane (bis-tris), binds to the "W" pocket mediated by a sodium ion (Fig. S7D). In contrast, the "R" pocket remains freely accessible. The surface charge network of TeNT/iH_C presents the face of
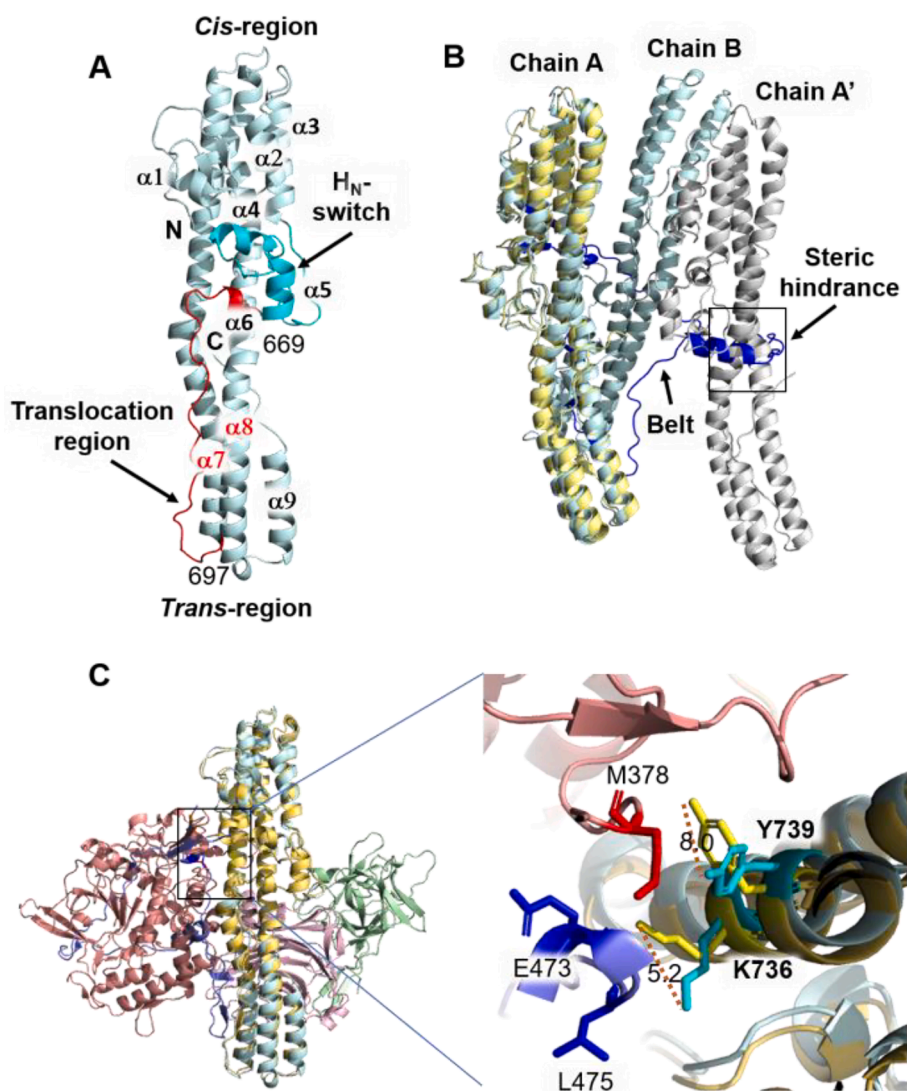
Fig. 2. Crystal structure of the isolated translocation domain of TeNT (TeNT/iH$_N$). (A) Crystal structure of TeNT/iH$_N$. The α helices in TeNT/iH$_N$ are labeled α1–9 from the N- to C-terminus. The H$_N$-switch (629–668) and translocation region (669–697) are colored in cyan and red, respectively. The part in the H$_N$ near the H$_N$-switch and C-terminal of the translocation region are termed the *Cis*-region and *Trans*-region, respectively. (B) Superimposition of rTeNT/H$_N$ (564–864, yellow) onto an isolated H$_N$ molecule (chain A) arranged in the crystal (pale cyan). The molecule (chain A') in the crystal packing of the neighboring asymmetric unit is shown in gray. The neighboring TeNT/iH$_N$ molecule sterically hinders the belt region (blue) in rTeNT/iH$_N$. (C) Superimposition of chain A of TeNT/iH$_N$ (564–864) onto rTeNT. The structural differences between TeNT/iH$_N$ and TeNT/H$_N$ were found at K736 and Y739. Interactions between TeNT/H$_N$ (yellow) and the Belt (blue) and LC (red) in rTeNT were disrupted in TeNT/iH$_N$ (cyan). (For interpretation of the references to colour in this figure legend, the reader is referred to the web version of this article.)

the receptor-binding site with a highly positive charge network, whereas the opposite face displays a highly negative charge network (Fig. S7E), suggesting that the positive charge network surface of the H$_C$ may interact closely with the negatively charged lipid membrane after binding to receptors.

We further compared the structure of TeNT/iH$_C$ with rTeNT/H$_C$ and nrTeNT/H$_C$ (Fig. S8A). A fluctuating loop (residues 981–987, termed the toggle loop) in the H$_{CN}$ of TeNT/iH$_C$ and rTeNT is well defined, whereas the corresponding loop in nrTeNT was not observed (Fig. S8B). The toggle loop in the H$_{CN}$ of rTeNT interacts with the H$_N$. The interactions include the D705–S984 hydrogen bond and an electrostatic interaction between E709 and K981. L985 in the toggle loop interacts with a hydrophobic patch in rTeNT/H$_N$, which is formed by I700, I832, I839 and L847. As a result, the translocation region in nrTeNT is likely to be stabilized and shortened by the interaction, leading to extended alpha helix 7 in rTeNT (Fig. S5C). In contrast, residues 938–942 form a flexible loop in rTeNT (termed 938loop) but form a short helix in nrTeNT (termed 938helix) with an electrostatic interaction between R802 and D940, and a hydrogen bond between S864 and D940 (Fig. S8C). In this sense, the domain rotation and structural rearrangement may optimize the positioning of the H$_C$ in TeNT, which favors proteinaceous receptor binding and formation of the C869–C1093 disulfide bond, as observed in nrTeNT.

3. Discussion

The molecular basis for the close cooperation of each domain during membrane translocation of TeNT/LC remains largely unknown in spite of vigorous structural studies on TeNT. Here, we have discovered that TeNT undergoes domain rotation via its own rotation linker and the Belt has a high propensity to swing around the upper half of TeNT/H$_N$ in the absence of the LC (Fig. S9A, Fig. 3). Due to rTeNT and nrTeNT were crystallized at pH 7.0 and 6.5, respectively, the observed domain rotations are unlikely to be caused by a difference in crystallization pH (Masuyer et al., 2017). Additionally, ligand binding does not seem to contribute to the observed domain reorganization because no significant conformational changes were observed in the homologous botulinum neurotoxin B (BoNT/B), in the presence and absence of a ligand (Swaminathan and Eswaramoorthy, 2000). A major difference between rTeNT and nrTeNT is that rTeNT was purified in the presence of TCEP, whereas no TCEP was present during the purification of nrTeNT. The absence of the tetanus-specific C869–C1093 disulfide bond in rTeNT indicates that the presence of the reductant TCEP has disrupted this surface exposed disulfide bond and led to domain rearrangement of TeNT (Fig. S2C-E). Similar domain reorganizations are reported in BoNTs, although they require formation of a complex, which is named the minimally functional-progenitor toxin complex (M-PTC), with a partner protein, the non-toxic non-hemagglutinin (NTNH) protein. For

Table 2
Data collection and statistical analysis of the solution structures.

	TeNT/iH$_N$	TeNT/blH$_N$
SASBDB ID	SASDJN5	SASDJP5
Guinier analysis		
$I(0)$ (cm^{-2})	0.012 ± 0.000032	0.014 ± 0.000046
R_g (Å)	30.35 ± 0.14	29.31 ± 0.16
q_{min} (Å^{-1})	0.011	0.012
qR_g max	1.29	1.29
Coefficient of correlation, R^2	0.71	0.91
Porod volume, V_p (Å^{-3})	70,410	52,186
M estimated from V_p (kDa)	44.0	32.6
$P(r)$ analysis		
$I(0)$ (cm^{-2})	0.01176 ± 0.0004347	0.01422 ± 0.0005349
R_g (Å)	32.24 ± 0.2473	31.38 ± 0.2272
D_{max} (Å)	121.32	112.16
χ^2 (total estimate from GNOM)	0.7908	0.7619
DAMMIN (13 independent calculations)		
q range for fitting (Å^{-1})	0.011–0.263	0.012–0.250
NSD (standard deviation)	0.017	0.012
χ^2 range	1.122–1.136	0.9660–0.9730
Resolution (from SASRES) (Å)	35 ± 3	31 ± 3
M estimate as volume of models (kDa)	45.2	36.2
DAMMIN (Final model built using the above merged model as a starting model)		
χ^2	1.122	0.9704
M estimate as volume of models (kDa)	45.2	36.2
EOM (Models of loop region of 459–573 generated with the compact-chain mode)		
χ^2, CORMAP P-value	1.266, 0.011	–
Constant subtraction	0	–
No. of representative structures	3	–

example, BoNT/A displays a linear domain organization in the free form, but changes its conformation by an ~ 140 degrees rotation of the H$_C$ in the M-PTC (Gu et al., 2012) (Fig. S9B). A conformation of the botulinum neurotoxin E (BoNT/E) in the M-PTC also undergoes a conformational change caused by rotation of the H$_C$ by ~ 60 degrees when compared with its apo-state BoNT/E domain organization (Eswaramoorthy et al., 2015) (Fig. S9C). In both BoNTs, the domain rotation is induced by the NTNH and via a linker between the H$_N$ and H$_{CN}$, which corresponds to the rotation linker in TeNT. The formation of the M-PTC of BoNT is hypothesized to facilitate delivery of the toxin across the intestinal epithelial barrier (Lam and Jin, 2015). However, after BoNT is released from the M-PTC at neutral or basic pH, the change in conformation of BoNT and how this conformational change relates to membrane translocation of the LC remains unresolved (Baldwin et al., 2007; Kumaran et al., 2009; Lam et al., 2015). In contrast, no partner protein that forms a M-PTC with TeNT has been reported. Therefore, domain reorganization in TeNT without an NTNH is likely to be associated with other biological roles, and the observed self-rotation of TeNT in this study may play a role in the membrane translocation of TeNT. Based on newly obtained structural information in present study, we propose a possible membrane translocation mechanism of TeNT (Fig. 4).

Taking that into account *C. tetani* is an anaerobic spore-forming bacterium; TeNT is likely to be produced as rTeNT initially. At the beginning of translocation, TeNT is in the reduced form and the rotation linker without the C869–C1093 disulfide bond is thought to be flexible. Such flexibility allows TeNT undergoes domain rotation. Because the translocation region is located on the opposite side to the GBS, it has to reorient to contact with the presynaptic membrane wall (Fig. 4A). Once the H$_C$ is anchored and domain rotation occurs on the membrane wall, the H$_N$ and LC locate closer to the presynaptic membrane, which is favorable for insertion of the translocation region into the lipid membrane, as presented in nrTeNT (Fig. 4B). Additionally, domain rotation enables TeNT to form a more compact state and promote translocation.

BoNT/E internalization and translocation is faster than any other BoNTs because of its unique compact domain organization (Kumaran et al., 2009). Comparison of the structures of rTeNT, nrTeNT and BoNT/E shows that nrTeNT is more compact than rTeNT but not as compact as BoNT/E (Fig. S10). The distance between the GBS and translocation region is shortest in BoNT/E and longest in rTeNT. These results indicate that nrTeNT is a transition state between the states observed in rTeNT (pre-translocation state) and BoNT/E (ready-for-translocation state).

The domain rotation also changes the region in the H$_C$ that interacts with the H$_N$, meaning that from the toggle loop in rTeNT to the 938helix in nrTeNT (Fig. S8B, C). C869 and C1093 move closer after domain reorganization, which promotes C869 to interact with C1093 and form the C869–C1093 disulfide bridge, as observed in nrTeNT (Fig. S8C). In fact, C869 has also been shown to be the primary residue involved in concentration-dependent disulfide formation of TeNT/iH$_C$ (Qazi et al., 2007). As a result, the H$_C$ could optimize its position in TeNT, which may induce an interaction between the H$_C$ and proteinaceous receptor, such as the SV2 (Yeh et al., 2010) and glycophosphatidylinositol (GPI)-anchored protein (Munro et al., 2001). Binding to a protein receptor, which follows the binding to a ganglioside, may also promote the interaction between the H$_C$ and membrane (Rummel et al., 2003). The face of the receptor-binding site with a highly positive charge network suggests that the H$_C$ could approach the membrane after binding to receptors (Fig. 4C).

To cleave VAMP2 in the cytosol of neuronal cells, the LC should be delivered from the synaptic vesicle lumen to the cytosol (Dong et al., 2019). This process is mediated by the H$_N$ upon endosome acidification (Fischer and Montal, 2013; Mushrush et al., 2011; Burns and Baldwin, 2014), which is generated by the vesicular ATPase proton pump (Williamson and Neale, 2002; Sun et al., 2012). The Belt in H$_N$ contains numerous negatively charged residues that will not favor interaction with the anionic membrane wall, thereby limiting the H$_N$-membrane interaction during membrane translocation of the LC (Galloux et al., 2008). The LC shows a high propensity to interact with and permeabilize anionic lipid bilayers upon acidification (Araye et al., 2016). Here, we found that the nrTeNT structure shows an extended translocation region (Fig. S5C). The acquired flexibility may facilitate interaction between the translocation region and membrane (Fig. 4C). In addition, the 333loop is found to be close to the translocation region (Fig. S3C) and may interact with the synaptic vesicle lumen upon H$_N$ membrane insertion. This is because the 333loop contains several negatively charged residues (Fig. S3D) that could be protonated (i.e., uncharged) at low pH, and this change in charge may enable hydrophobic interactions between the LC and lipid bilayer (Araye et al., 2016). However, the direct evidence of the interactions between the 333loop and lipid bilayer as a function of pH remains to be validated.

We have uncovered the movement of the Belt in an isolated H$_N$ construct at acidic pH (pH 6.0); the Belt has a high propensity to swing around the upper half of iH$_N$ in solution (Fig. 3). Moreover, a beltless H$_N$ of BoNT/A, the buried α-helices transform into surface-exposed hydrophobic β-hairpins triggered by acidic pH, which promotes membrane insertion of the H$_N$ (Lam et al., 2018). At low pH, numerous negative charges in the Belt and LC likely to be neutralized because of side chain protonation, and may result in weak interactions between the Belt and LC. Thus, the Belt is released upon a decrease in the pH, which could weaken electrostatic repulsions between the H$_N$ and synaptic vesicle lumen, allowing its penetration into the membrane (Galloux et al., 2008). And the loop (residues 762–769) moves dramatically, which may be involved in the LC translocation by adjusting the LC for transmembrane insertion (Zuverink et al., 2020), because the loop is located in close proximity to the C439–C476 disulfide bond. This disulfide bond was shown previously to be needed for membrane translocation of the LC (Montecucco, 1990; Zuverink et al., 2015). The LC has been shown to undergo a secondary structure change when on an anionic membrane under acidic pH conditions (Fu et al., 2002). Presumably, under low pH and negatively charged lipid membrane conditions, the H$_N$ and LC may
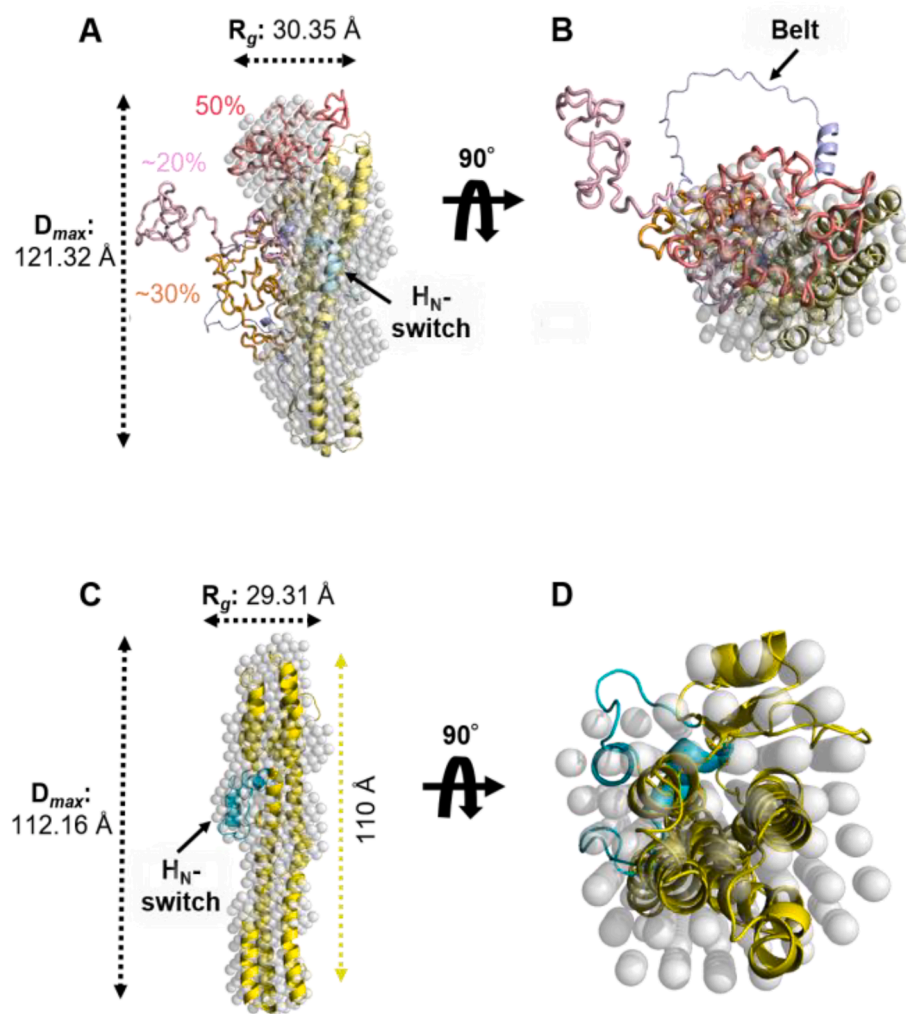
Fig. 3. Solution structures of TeNT/iH$_N$ and TeNT/blH$_N$. (A, B) The crystal structure and EOM models (cartoon representation) of rTeNT/H$_N$ was fitted into the ben rod part of the DAMMIN model (gray, beads representation) of TeNT/iH$_N$. (A) and (B) present front and top views, respectively. The radius of gyration (R_g) and the maximum intramolecular distance (D_{max}) were 30.35 and 121.32 Å, respectively. The non-negligible unfitted additional parts were observed around rTeNT/H$_N$, representing the location of the Belt in the solution structure of TeNT/iH$_N$. The abundance of each EOM model was 50% (salmon), 30% (orange) and 20% (pink), respectively. (C, D) The crystal model of rTeNT/blH$_N$ (564–864) was fitted into the rod-like shape DAMMIN model (gray, beads representation) of TeNT/blH$_N$. (C) and (D) present front and top views, respectively. The R_g and D_{max} were 29.31 and 112.16 Å, respectively. The value of D_{max} is close to the 110 Å observed in the TeNT/iH$_N$ crystal structure. The crystal model of rTeNT/blH$_N$ fitted well into beads model of TeNT/blH$_N$.

adopt molten globule states (Pirazzini et al., 2016), which conserves a native-like secondary structure content but without a tightly packed tertiary fold. Considering these points, we propose that LC anchoring to the endosomal membrane may cause the belt to swing around the upper half of the H$_N$, which likely facilitate the conformational change of the H$_N$ to enable formation of a cleft in the vesicle lumen for LC delivery (Fig. 4D) (Rossetto et al., 2014). Intermediate state of the membrane translocation of the LC is not clear, and the visualization of TeNT-endosomal membrane interaction is highly desired. Once exposed to the cytosolic environment, the C439–C467 disulfide bond connecting the H$_N$ and LC is reduced by a thioredoxin reductase-thioredoxin system in the neuron cytosol (Montecucco, 1990).

4. Conclusions

We have investigated the structural flexibility of TeNT by crystallographic and solution scattering analyses. While all CNTs share the rotation linker as a player for domain rearrangement, the evolution of TeNT has chosen a unique disulfide bond switch that controls domain rotation. Crystal structure and solution structure analysis of TeNT/iH$_N$ provides the first overview of the dynamics of the Belt in solution (regardless of the absence of LC and membrane). These structural insights provide hints for the development of new inhibitors (small-molecule or peptide/antibody) that prevent TeNT poisoning. The TeNT could also be used for alternative applications. For example, in neurodegenerative diseases, coupling of protein-based therapeutics to a

modified non-toxic TeNT complex/chimera could regulate drug delivery in a time- and location-dependent manner to ensure maximum performance.

5. Materials and methods

DNA construction, protein expression, purification and crystallization of rTeNT, TeNT/iH$_N$ and TeNT/iH$_C$ are described in the Appendix A. Supplementary data. Structural insights were studied by crystallography and small angle X-ray scattering. Data collection of crystal and solution structures was performed at beamline BL44XU and BL45XU, respectively, of the super photon ring-8 GeV (Spring-8). Processing of data and structural analysis was performed as described in the Appendix A. Supplementary data.

6. Data availability

Atomic coordinates and structure factors for rTeNT, TeNT/iH$_N$ and TeNT/iH$_C$ have been deposited in the Protein Data Bank under accession codes 7BY5, 7BXX and 7BY4, respectively. For 7BXX, the final pdb coordinates was deposited at RCSB PDB on September 1, 2020. Solution structure factors for TeNT/iH$_N$ and TeNT/blH$_N$ have been deposited in the Small Angle Scattering Biological Data Bank under accession codes SASDJN5 and SASDJP5, respectively.
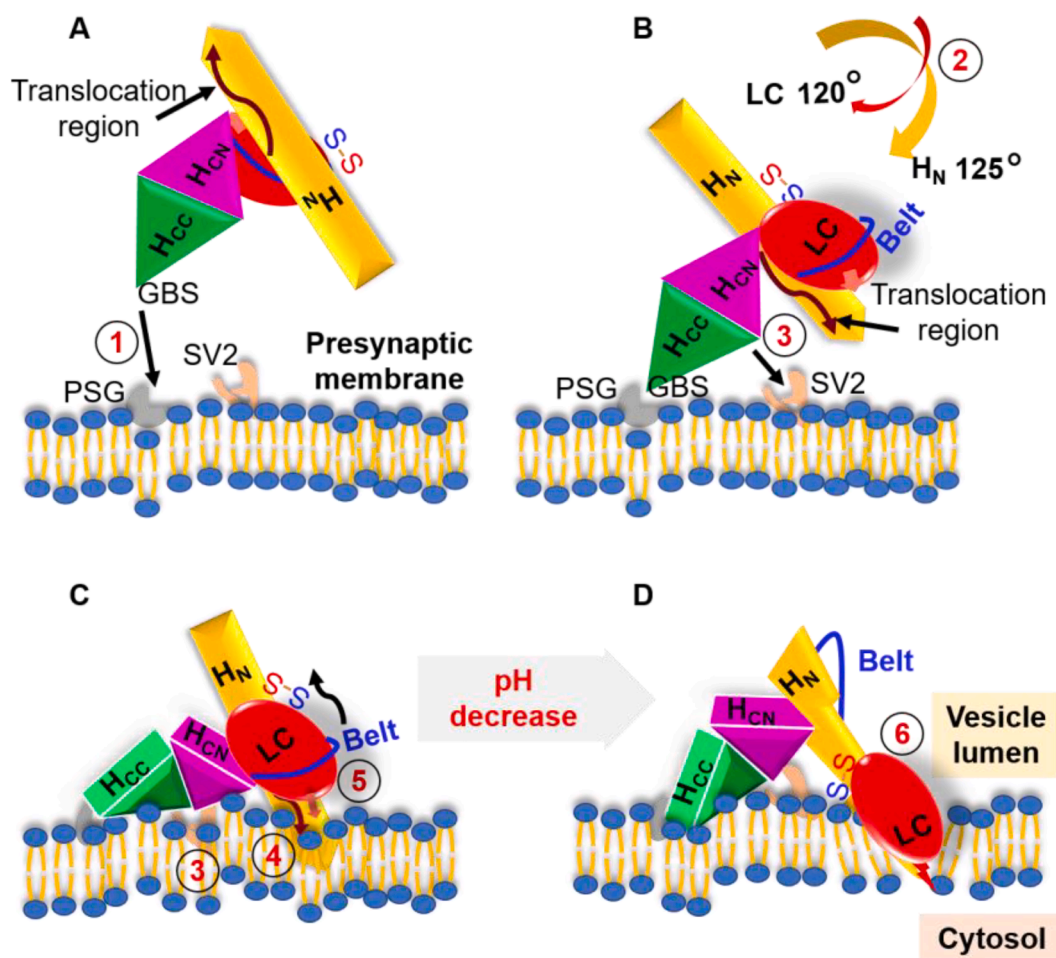
Fig. 4. Schematic model of the potential membrane translocation mechanism of TeNT. (A) Receptor binding of TeNT on the membrane wall. Before anchoring to the membrane by the H_{CC} (green), the GBS in flexible rTeNT/H_{CC} searches for the PSG (gray illustration) on the membrane (A-①). The H_N (yellow big arrow) and LC (red ellipse) are distal from the membrane and the transmembrane region (dark red long arrow) is on the vertical side of the GBS. (B) Domain rotation of the H_N and LC. Domains rotate in rTeNT after binding to the membrane via the H_{CC} (B-②). This domain rotation and structural rearrangement leads to the H_N and LC positioning closer to the membrane along with the transmembrane region. (C) The formation of ready-for-translocation state. TeNT/H_C binds to proteinaceous receptor, such as the SV2 (brown illustration) (C-③). The acquired flexibility of the translocation region is desirable for its membrane interaction (C-④). The LC interacts with the lipid bilayer (C-⑤) and the Belt show electrostatic repulsion toward the anionic membrane (black curved arrow). (D) Membrane translocation of the LC. Secondary structure changes of the H_N and LC on the anionic membrane upon a decrease in pH. The Belt swings around the upper half of H_N, and the LC is delivered into cytosol through the delivery device (D-⑥). (For interpretation of the references to colour in this figure legend, the reader is referred to the web version of this article.)

CRediT authorship contribution statement

Chun-ming Zhang: Investigation, Conceptualization, Methodology, Writing - original draft, Writing - review & editing, Visualization. **Yoshihiro Imoto:** Investigation, Conceptualization, Methodology, Writing - original draft, Visualization. **Takaaki Hikima:** Methodology, Writing - original draft, Writing - review & editing, Visualization. **Tsuyoshi Inoue:** Funding acquisition, Project administration, Conceptualization, Supervision, Writing - original draft, Writing - review & editing.

Declaration of Competing Interest

The authors declare that they have no known competing financial interests or personal relationships that could have appeared to influence the work reported in this paper.

Appendix A. Supplementary data

Supplementary data to this article can be found online at https://doi.org/10.1016/j.yjsbx.2021.100045.

References

Araye, A., Goudet, A., Barbier, J., Pichard, S., Baron, B., England, P., Pérez, J., Zinn-Justin, S., Chenal, A., Gillet, D., 2016. The translocation domain of botulinum neurotoxin A moderates the propensity of the catalytic domain to interact with membranes at acidic pH. PLoS One 11. https://doi.org/10.1371/journal.pone.0153401.

Baldwin, M.R., Kim, J.-J.P., Barbieri, J.T., 2007. Botulinum neurotoxin B–host receptor recognition: it takes two receptors to tango. Nat. Struct. Mol. Biol. 14, 9–10. https://doi.org/10.1038/nsmb0107-9.

Bercsenyi, K., Schmieg, N., Bryson, J.B., Wallace, M., Caccin, P., Golding, M., Zanotti, G., Greensmith, L., Nischt, R., Schiavo, G., 2014. Nidogens are therapeutic targets for the prevention of tetanus. Science 346, 1118–1123. https://doi.org/10.1126/science.1258138.

Bordet, T., Castelnau-Ptakhine, L., Fauchereau, F., Friocourt, G., Kahn, A., Haase, G., 2001. Neuronal targeting of cardiotrophin-1 by coupling with tetanus toxin C fragment. Mol. Cell Neurosci. 17, 842–854. https://doi.org/10.1006/mcne.2001.0979.

Bruggemann, H., Baumer, S., Fricke, W. F., Wiezer, A., Liesegang, H., Decker, I., Herzberg, C., Martinez-Arias, R., Merkl, R., Henne, A. & Gottschalk, G. (2003) The genome sequence of Clostridium tetani, the causative agent of tetanus disease, Proc Natl Acad Sci USA. 100, 1316-1321. DOI: 10.1073/pnas.0335853100.

Burns, J.R., Baldwin, M.R., 2014. Tetanus neurotoxin utilizes two sequential membrane interactions for channel formation. J. Biol. Chem. 289, 22450–22458. https://doi.org/10.1074/jbc.m114.559302.

Chen, C., Fu, Z., Kim, J.-J.P., Barbieri, J.T., Baldwin, M.R., 2009. Gangliosides as high affinity receptors for tetanus neurotoxin. J. Biol. Chem. 284, 26569–26577. https://doi.org/10.1074/jbc.m109.027391.

Coen, L., Osta, R., Maury, M., Brulet, P., 1997. Construction of hybrid proteins that migrate retrogradely and transynaptically into the central nervous system. Proc. Natl. Acad. Sci. U.S.A. 94, 9400–9405. https://doi.org/10.1073/pnas.94.17.9400.

Dobrenis, K., Joseph, A., Rattazzi, M.C., 1992. Neuronal lysosomal enzyme replacement using fragment C of tetanus toxin. Proc. Nati. Acad. Sci. U.S.A. 89, 2297–2301. https://doi.org/10.1073/pnas.89.6.2297.

Dong, M., Masuyer, G., Stenmark, P., 2019. Botulinum and tetanus neurotoxins. Annu. Rev. Biochem. 88, 811–837. https://doi.org/10.1146/annurev-biochem-013118-111654.

Eisel, U., Jarausch, W., Goretzki, K., Henschen, A., Engels, J., Weller, U., Hudel, M., Habermann, E., Niemann, H., 1986. Tetanus toxin: primary structure, expression in E. coli, and homology with botulinum toxins. EMBO J. 5, 2495–2502. https://doi.org/10.1002/j.1460-2075.1986.tb04527.x.

Eswaramoorthy, S., Sun, J., Li, H., Singh, B.R., Swaminathan, S., 2015. Molecular assembly of clostridium botulinum progenitor M complex of type E. Sci. Rep. 5, 17795. https://doi.org/10.1038/srep17795.

Fischer, A., Montal, M., 2013. Molecular dissection of botulinum neurotoxin reveals interdomain chaperone function. Toxicon 75, 101–107. https://doi.org/10.1016/j.toxicon.2013.01.007.

Fischer, A., Sambashivan, S., Brunger, A.T., Montal, M., 2012. Beltless translocation domain of botulinum neurotoxin A embodies a minimum ion-conductive channel. J. Biol. Chem. 287, 1657–1661. https://doi.org/10.1074/jbc.c111.319400.

Fu, F.-N., Busath, D.D., Singh, B.R., 2002. Spectroscopic analysis of low pH and lipid-induced structural changes in type A botulinum neurotoxin relevant to membrane channel formation and translocation. Biophys. Chem. 99, 17–29. https://doi.org/10.1016/s0301-4622(02)00135-7.

Galloux, M., Vitrac, H., Montagner, C., Raffestin, S., Popoff, M.R., Chenal, A., Forge, V., Gillet, D., 2008. Membrane interaction of botulinum neurotoxin A Translocation (T) Domain: the belt region is a regulatory loop for membrane interaction. J. Biol. Chem. 283, 27668–27676. https://doi.org/10.1074/jbc.m802557200.

Gu, S., Rumpel, S., Zhou, J., Strotmeier, J., Bigalke, H., Perry, K., Shoemaker, C.B., Rummel, A., Jin, R., 2012. Botulinum neurotoxin is shielded by NTNHA in an interlocked complex. Science 335, 977–981. https://doi.org/10.1126/science.1214270.

Hesse, S., Kutschenko, A., Bryl, B., Deutschland, M., Liebetanz, D., 2020. Therapeutic effects of Tetanus neurotoxin in spinal cord injury: a case series on four dogs. Spinal Cord Series Cases 6. https://doi.org/10.1038/s41394-020-0258-9.

Kissa, K., 2002. In vivo neuronal tracing with GFP-TTC gene delivery. Mol. Cell Neurosci. 20, 627–637. https://doi.org/10.1006/mcne.2002.1141.

Kumaran, D., Eswaramoorthy, S., Furey, W., Navaza, J., Sax, M., Swaminathan, S., 2009. Domain organization in clostridium botulinum neurotoxin type E is unique: its implication in faster translocation. J. Mol. Biol. 386, 233–245. https://doi.org/10.1016/j.jmb.2008.12.027.

Lam, K.-H., Jin, R., 2015. Architecture of the botulinum neurotoxin complex: a molecular machine for protection and delivery. Curr. Opin. Struct. Biol. 31, 89–95. https://doi.org/10.1016/j.sbi.2015.03.013.

Lam, K.-H., Yao, G., Jin, R., 2015. Diverse binding modes, same goal: the receptor recognition mechanism of botulinum neurotoxin. Prog. Biophys. Mol. Biol. 117, 225–231. https://doi.org/10.1016/j.pbiomolbio.2015.02.004.

Lam, K.-H., Guo, Z., Krez, N., Matsui, T., Perry, K., Weisemann, J., Rummel, A., Bowen, M.E., Jin, R., 2018. A viral-fusion-peptide-like molecular switch drives membrane insertion of botulinum neurotoxin A1. Nature Commun. 9 https://doi.org/10.1038/s41467-018-07789-4.

Maskos, U., Kissa, K., St. Cloment, C., Brulet, P., 2002. Retrograde trans-synaptic transfer of green fluorescent protein allows the genetic mapping of neuronal circuits in transgenic mice. Proc. Natl. Acad. Sci. U.S.A. 99, 10120–10125. https://doi.org/10.1073/pnas.152266799.

Masuyer, G., Conrad, J., Stenmark, P., 2017. The structure of the tetanus toxin reveals pH-mediated domain dynamics. EMBO Rep. 18, 1306–1317. https://doi.org/10.15252/embr.201744198.

Montal, M., 2009. Translocation of botulinum neurotoxin light chain protease by the heavy chain protein-conducting channel. Toxicon 54, 565–569. https://doi.org/10.1016/j.toxicon.2008.11.018.

Montecucco, C., 1990. An intact interchain disulfide bond is required for the neurotoxicity of tetanus toxin. Infection Immunity 58, 4136–4141. https://doi.org/10.1128/iai.58.12.4136-4141.1990.

Moreno-Martinez, Laura, 2020. Neuroprotective Fragment C of Tetanus Toxin Modulates IL-6 in an ALS Mouse Model. Toxins (Basel). https://doi.org/10.3390/toxins12050330.

Munro, P., Kojima, H., Dupont, J.-L., Bossu, J.-L., Poulain, B., Boquet, P., 2001. High sensitivity of mouse neuronal cells to tetanus toxin requires a GPI-anchored protein. BBRC 289, 623–629. https://doi.org/10.1006/bbrc.2001.6031.

Mushrush, D.J., Koteiche, H.A., Sammons, M.A., Link, A.J., McHaourab, H.S., Lacy, D.B., 2011. Studies of the Mechanistic Details of the pH-dependent Association of Botulinum Neurotoxin with Membranes. J Biol Chem 286, 27011–27018. https://doi.org/10.1074/jbc.m111.256982.

Oblatt-Montal, M., Yamazaki, M., Nelson, R., Montal, M., 1995. Formation of ion channels in lipid bilayers by a peptide with the predicted transmembrane sequence of botulinum neurotoxin A. Protein Sci. 4, 1490–1497. https://doi.org/10.1002/pro.5560040806.

Payne, A.M., Zheng, Z., Messi, M.L., Milligan, C.E., González, E., Delbono, O., 2006. Motor neurone targeting of IGF-1 prevents specific force decline in ageing mouse muscle. J. Physiol. 570, 283–294. https://doi.org/10.1113/jphysiol.2005.100032.

Pirazzini, M., Rossetto, O., Bolognese, P., Shone, C.C., Montecucco, C., 2011. Double anchorage to the membrane and intact inter-chain disulfide bond are required for the low pH induced entry of tetanus and botulinum neurotoxins into neurons. Cell Microbiol. 13, 1731–1743. https://doi.org/10.1111/j.1462-5822.2011.01654.x.

Pirazzini, M., Tehran, D.A., Leka, O., Zanetti, G., Rossetto, O., Montecucco, C., 2016. On the translocation of botulinum and tetanus neurotoxins across the membrane of acidic intracellular compartments. Biochim. Biophys. Acta 1858, 467–474. https://doi.org/10.1016/j.bbamem.2015.08.014.

Qazi, O., Bolgiano, B., Crane, D., Svergun, D.I., Konarev, P.V., Yao, Z.-P., Robinson, C.V., Brown, K.A., Fairweather, N., 2007. The HC fragment of tetanus toxin forms stable, concentration-dependent dimers via an intermolecular disulphide bond. J. Mol. Biol. 365, 123–134. https://doi.org/10.1016/j.jmb.2006.09.050.

Rind, H.B., 2005. Synaptic targeting of retrogradely transported trophic factors in motoneurons: comparison of glial cell line-derived neurotrophic factor, brain-derived neurotrophic factor, and cardiotrophin-1 with Tetanus Toxin. J. Neurosci. 25, 539–549. https://doi.org/10.1523/jneurosci.4322-04.2005.

Rossetto, O., Pirazzini, M., Montecucco, C., 2014. Botulinum neurotoxins: genetic, structural and mechanistic insights. Nature Rev. Microbiol. 12, 535–549. https://doi.org/10.1038/nrmicro3295.

Rossetto, O., Pirazzini, M., Lista, R., Montecucco, C., 2019. The role of the single interchains disulfide bond in Tetanus and Botulinum Neurotoxins and the development of anti-tetanus and anti-botulism drugs. Cell Microbiol. e13037 https://doi.org/10.1111/cmi.13037.

Roux, S., Saint Cloment, C., Curie, T., Girard, E., Mena, F.-J.M., Barbier, J., Osta, R., Molgó, J., Brûlet, P., 2006. Brain-derived neurotrophic factor facilitates in vivo internalization of tetanus neurotoxin C-terminal fragment fusion proteins in mature mouse motor nerve terminals. Eur. J. Neurosci. 24, 1546–1554. https://doi.org/10.1111/j.1460-9568.2006.05030.x.

Rummel, A., Bade, S., Alves, J., Bigalke, H., Binz, T., 2003. Two carbohydrate binding sites in the HCC-domain of tetanus neurotoxin are required for toxicity. J. Mol. Biol. 326, 835–847. https://doi.org/10.1016/s0022-2836(02)01403-1.

Schiavo, G.G., Benfenati, F., Poulain, B., Rossetto, O., De Laureto, P.P., Dasgupta, B.R., Montecucco, C., 1992. Tetanus and botulinum-B neurotoxins block neurotransmitter release by proteolytic cleavage of synaptobrevin. Nature 359, 832–835. https://doi.org/10.1038/359832a0.

Schiavo, G., Matteoli, M., Montecucco, C., 2000. Neurotoxins affecting neuroexocytosis. Physiol. Rev. 80, 717–766. https://doi.org/10.1152/physrev.2000.80.2.717.

Schwab, M., 1979. Selective retrograde transsynaptic transfer of a protein, tetanus toxin, subsequent to its retrograde axonal transport. J. Cell Biol. 82, 798–810. https://doi.org/10.1083/jcb.82.3.798.

Südhof, T.C., Jahn, R., 1991. Proteins of synaptic vesicles involved in exocytosis and membrane recycling. Neuron 6, 665–677. https://doi.org/10.1016/0896-6273(91)90165-v.

Sun, S., Tepp, W.H., Johnson, E.A., Chapman, E.R., 2012. Botulinum neurotoxins B and E translocate at different rates and exhibit divergent responses to GT1b and low pH. Biochemistry 51, 5655–5662. https://doi.org/10.1021/bi3004928.

Swaminathan, S., Eswaramoorthy, S., 2000. Structural analysis of the catalytic and binding sites of Clostridium botulinum neurotoxin B. Nat. Struct. Mol. Biol. 7, 693–699. https://doi.org/10.1038/78005.

Toivonen, J.M., Oliván, S., Osta, R., 2010. Tetanus toxin C-fragment: the courier and the cure? Toxins (Basel) 2, 2622–2644. https://doi.org/10.3390/toxins2112622.

WHO, Protecting all against tetanus, 2019. ISBN: 9789241515610. The date of last accessed: 28 Aug. 2020. https://apps.who.int/iris/bitstream/handle/10665/329882/9789241515610-eng.pdf?ua=1.

Williamson, L.C., Neale, E.A., 2002. Bafilomycin A1 inhibits the action of tetanus toxin in spinal cord neurons in cell culture. J. Neurochem. 63, 2342–2345. https://doi.org/10.1046/j.1471-4159.1994.63062342.x.

Yeh, F.L., Dong, M., Yao, J., Tepp, W.H., Lin, G., Johnson, E.A., Chapman, E.R., 2010. SV2 mediates entry of tetanus neurotoxin into central neurons. PLoS Pathogens 6. https://doi.org/10.1371/journal.ppat.1001207.

Zuverink, M., Chen, C., Przedpelski, A., Blum, F.C., Barbieri, J.T., 2015. A heterologous reporter defines the role of the tetanus toxin interchain disulfide in light-chain translocation. Infection Immunity 83, 2714–2724. https://doi.org/10.1128/iai.00477-15.

Zuverink, M., Bluma, M., Barbieri, J.T., 2020. Tetanus toxin cis-loop contributes to light-chain translocation. mSphere. https://doi.org/10.1128/mSphere.00244-20.